Research Article

Nano Research
2020, 13(12): 3230–3234

ISSN 1998-0124 CN 11-5974/O4
https://doi.org/10.1007/s12274-020-2993-4

Inorganic/polymer hybrid layer stabilizing anode/electrolyte interfaces in solid-state Li metal batteries

Yiran Hu[1,2], Yiren Zhong[2], Limin Qi[1] (✉), and Hailiang Wang[2] (✉)

[1] *Beijing National Laboratory for Molecular Sciences (BNLMS), College of Chemistry and Molecular Engineering, Peking University, Beijing 100871,China*

[2] *Department of Chemistry and Energy Sciences Institute, Yale University, West Haven, CT 06516, USA*

Received: 2 June 2020 / **Revised:** 17 July 2020 / **Accepted:** 19 July 2020

ABSTRACT

$Li_{1.5}Al_{0.5}Ge_{1.5}(PO_4)_3$ (LAGP) is a solid-state electrolyte with high ionic conductivity and air stability but poor chemical stability and high interfacial impedance when directly contacted with Li metal. In this work, we develop an inorganic/polymer hybrid interlayer composed of Li bis(trifluoromethylsulfonyl)imide/poly(vinylene carbonate) polymer electrolyte and SiO_2 submicrospheres to stabilize the Li/LAGP interface. The polymeric component renders high ionic conductance and low interfacial resistance, whereas the inorganic component imparts flame retardancy and a physical barrier to the known Li-LAGP side reaction, together enabling stable Li stripping/plating for more than 1,500 h at room temperature. With this interlayer at both electrodes, all-solid-state Li||$LiFePO_4$ full cells with stable cycling performance are also demonstrated.

KEYWORDS

$Li_{1.5}Al_{0.5}Ge_{1.5}(PO_4)_3$ (LAGP), hybrid interlayer, solid-state electrolyte, Li metal battery, interface

Solid-state electrolytes are receiving extensive attention in battery applications because of their better safety compared to the conventional organic liquid electrolytes [1, 2]. Inorganic ceramics, such as NASICON-type [3–7], sulfide [8–11], perovskite-type [12, 13], and garnet-type [14–17] materials, with high ionic conductivity and mechanical strength, are promising solid-state electrolytes for safe and high-energy-density Li batteries. However, these electrolytes face issues including high solid/solid interfacial resistance and poor chemical stability in contact with electrode materials [18–20], which limit the development of solid-state batteries. For example, NASICON-type $Li_{1.4}Al_{0.4}Ti_{1.6}(PO_4)_3$ (LATP) [21–23] and $Li_{1.5}Al_{0.5}Ge_{1.5}(PO_4)_3$ (LAGP) [24–32] have good ionic conductivity (10^{-4}–10^{-3} S·cm^{-1}) and air stability, but are chemically unstable against Li metal, which cause poor cycling stability. Studies have shown that the degradation mechanism of LAGP involves its reduction by Li resulting in high interfacial resistance and cracking/pulverization of the electrolyte [30–34].

Because of the side reactions, Li|LAGP|Li cells without interfacial modification can only be cycled for less than 150 h at 0.1 mA·cm^{-2} with a high overpotential (> 300 mV) [30, 31, 33, 35]. Constructing an interlayer between Li and LAGP has emerged as a simple yet effective strategy for mitigating this problem. Both inorganic and polymeric materials have been used as interlayers [32, 36–42]. For example, a Ge thin film was sputtered on LAGP surface to suppress reduction of LAGP and improve its wettability for Li metal [38]. The resulting symmetrical cell could be cycled for 200 h at 0.1 mA·cm^{-2} before the Ge protective layer was consumed. Some studies introduced gel polymer electrolytes as interlayers between LAGP and Li [25–27, 29, 43, 44]. While these polymer interlayers are effective in extending battery cycle life, they compromise safety because of their thermal instability and even flammability. In order to further improve LAGP-based solid-state Li metal batteries, it is important to explore alternative interface protection methods.

In this work, we developed a composite interlayer consisting of SiO_2 submicrospheres embedded in a polymer electrolyte of Li bis(trifluoromethylsulfonyl)imide/poly(vinylene carbonate) (LiTFSI/PVCA) for LAGP-based solid-state Li batteries. In the composite structure, the polymer electrolyte component reduces the solid/solid interfacial resistance between the LAGP electrolyte and the Li metal electrode, and builds up ionically conductive channels between them (Fig. 1). The SiO_2 component physically separates LAGP from Li to prevent direct reaction of the solid electrolyte. As an inorganic filler, the SiO_2 submicrospheres also reduce the amount of polymer electrolyte necessary for forming an effective interlayer and enhance

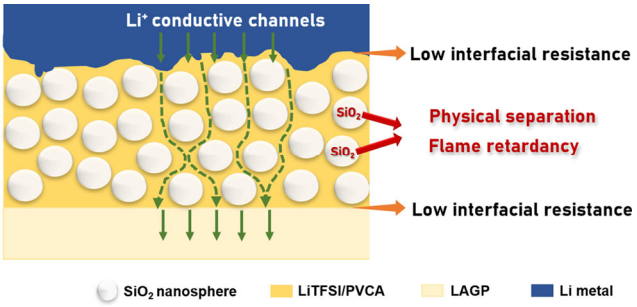

Figure 1 Design principle of PVCA–SiO_2 interlayer for stabilizing Li/LAGP interface.

Address correspondence to Limin Qi, liminqi@pku.edu.cn; Hailiang Wang, hailiang.wang@yale.edu

flame retardancy of the composite interlayer (Fig. 1), which could benefit battery safety. With the cooperation of these two components, this interlayer enables Li|LAGP|Li cells with an initial overpotential of 102 mV at 0.1 mA·cm^{-2} and can be stably cycled for over 1,500 h.

LAGP was synthesized via a solid-state reaction (see the Electronic Supplementary Material (ESM) for details) [38]. The resulting powder was then pressed and sintered into dense pellets with a thickness of 400–500 μm. Both the powder (Fig. S1 in the ESM) and pellet (Fig. S2 in the ESM) have a well-defined $LiGe_2(PO_4)_3$ crystal structure (PDF #: 80-1923) as revealed by X-ray diffraction (XRD). Li|LAGP|Li coin cells were assembled without using any interlayer at the electrode/electrolyte interfaces. Charged and discharged to a capacity of 0.1 mA·h·cm^{-2} at a constant current density of 0.1 mA·cm^{-2}, the cell maintained an overpotential of 300 mV for 100 h before the voltage hysteresis surged (Fig. 2(a)). The cycled LAGP pellet was found to be fractured and even partially pulverized with black species covering the surface (Fig. 2(b)). Scanning electron microscopy (SEM) images of the LAGP pellet revealed formation of metallic Li in the electrolyte bulk (Fig. 2(c)) and side reaction products on the surface (Fig. S3(a) in the ESM). X-ray photoelectron spectroscopy (XPS) measurement showed that at least part of the Ge (IV) on the electrolyte surface had been reduced to Ge (III) (Fig. 2(d)). The peak area ratio of Ge (III)/Ge (IV) is about 33%. The XRD pattern of the cycled pellet (Fig. S4(a) in the ESM) shows additional peaks in the range of 20°–26° (Fig. S4(b) in the ESM), which correspond to possible decomposition products, such as $LiAlGe_2O_6$, Li_3AlGeO_5, Li_3PO_4, and $AlPO_4$ [34, 45, 46]. Taken together, these results suggest that substantial side reactions take place at the direct-contact interface of LAGP and Li, which forms an interphase of high resistance to ionic transport and leads to Li penetration into the electrolyte bulk fracturing the pellet (Fig. 2(e)).

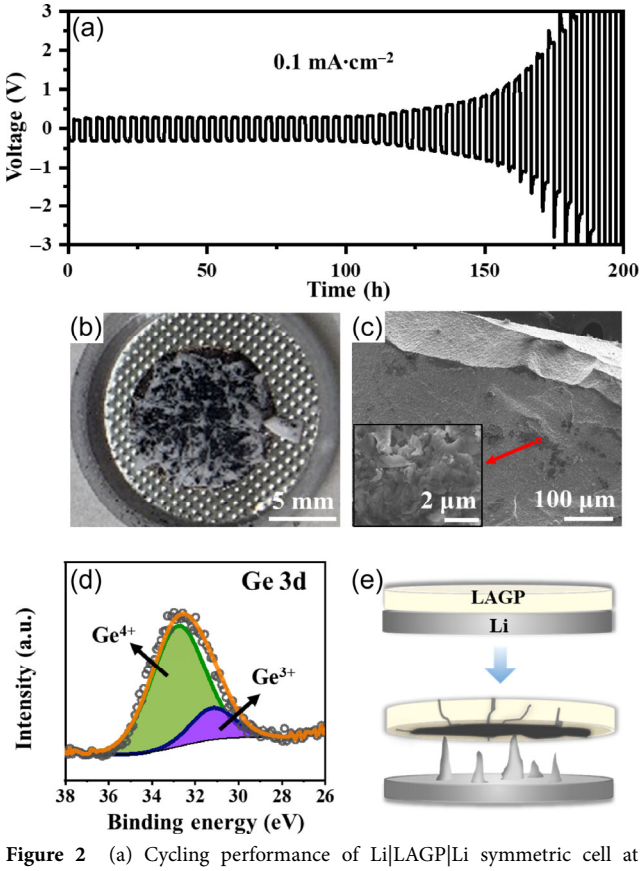

Figure 2 (a) Cycling performance of Li|LAGP|Li symmetric cell at 0.1 mA·cm^{-2} (current density)-0.1 mA·h·cm^{-2} (capacity). (b) Photograph and (c) low-magnification cross section SEM image of the LAGP pellet from the Li|LAGP|Li cell after 200 h of cycling at 0.1 mA·cm^{-2} (current density)-0.1 mA·h·cm^{-2} (capacity). The dark areas in (c) correspond to deposited Li in the LAGP pellet, with the inset showing a magnified area. (d) Ge 3d XPS of the surface of the cycled LAGP pellet. (e) Schematic illustration of side reactions and Li dendrite formation at direct-contact Li/LAGP interface.

To protect LAGP against Li and simultaneously ensure a good ionic contact between them, we first studied a PVCA polymer electrolyte as an interlayer (Fig. S5(a) in the ESM). The polymer electrolyte was prepared from LiTFSI and vinylene carbonate (VC) following a two-step polymerization process [47] and sandwiched between Li and LAGP with an amount of 17 μL·cm^{-2}. Charged and discharged under 0.1 mA·cm^{-2} (current density)-0.1 mA·h·cm^{-2} (capacity) conditions, the Li|PVCA|LAGP|PVCA|Li cell displayed a decreased initial overpotential of 115 mV compared to the Li|LAGP|Li cell (Fig. 3(a)). The cycle life was also extended to 500 h with the overpotential gradually increased to 405 mV at the end of cycling (Fig. 3(a)). The cycled LAGP pellet was fractured with black species observed on the surface and broken cross sections (Fig. 3(b)), which was also confirmed by SEM images (Fig. 3(c) and Fig. S3(b) in the ESM). XPS results showed that part of the Ge (IV) on the surface was reduced (Fig. 3(d)). The area ratio of Ge (III)/Ge (IV) is about 21%, lower than what was observed for the cycled Li|LAGP|Li cell. Based on these results, we conclude that the PVCA interlayer is effective in reducing the interfacial resistance between Li and LAGP but is not sufficient to prevent the side reactions between them (Fig. 3(e)). Consistently, Li||Li cells using LiTFSI/PVCA as electrolyte (without LAGP)

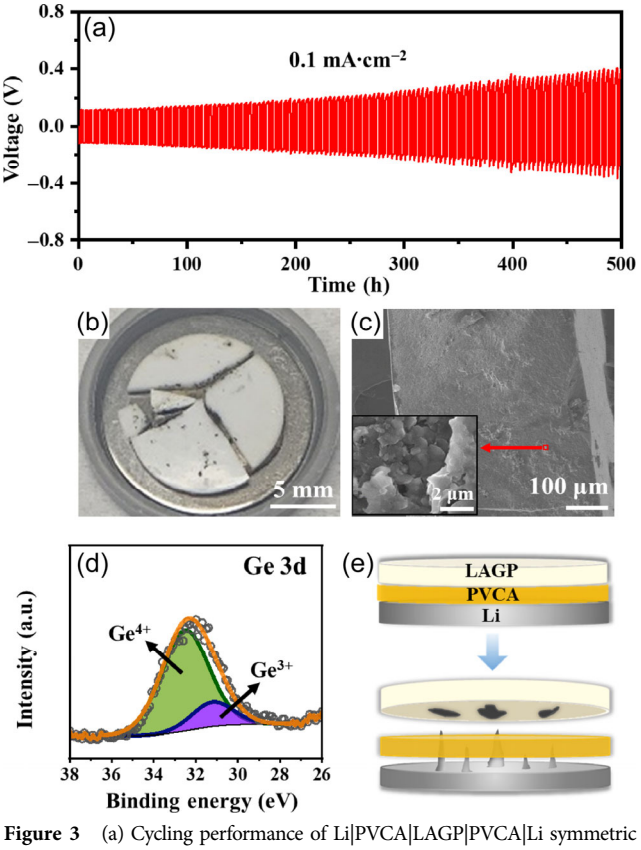

Figure 3 (a) Cycling performance of Li|PVCA|LAGP|PVCA|Li symmetric cell at 0.1 mA·cm^{-2} (current density)-0.1 mA·h·cm^{-2} (capacity). (b) Photograph of the LAGP pellet from the Li|PVCA|LAGP|PVCA|Li cell after 500 h of cycling at 0.1 mA·cm^{-2} (current density)-0.1 mA·h·cm^{-2} (capacity). (c) Low-magnification and (inset) magnified SEM images of a cross section of the cycled pellet. (d) Ge 3d XPS of the surface of the cycled LAGP pellet. (e) Schematic illustration of alleviated side reactions between Li and LAGP with PVCA interlayer.

showed an overpotential of 100 mV under 0.1 mA·cm^{-2} (current density)-0.1 mA·h·cm^{-2} (capacity) cycling conditions but short-circuited after only 80 h (Fig. S6 in the ESM).

To solve the remaining problem, we synthesized SiO_2 submicrospheres with a well-controlled diameter of about 800 nm (Fig. S7 in the ESM) [48] and blended them into the PVCA polymer electrolyte to prepare a new interlayer (Fig. S5(b) in the ESM). Charged and discharged under 0.1 mA·cm^{-2} (current density)-0.1 mA·h·cm^{-2} (capacity) conditions, the Li|PVCA–SiO_2|LAGP|PVCA–SiO_2|Li cell showed an initial overpotential of 102 mV and an excellent cycling stability for 1,500 h with a moderate increase of overpotential to 250 mV (Fig. 4(a)). This is among the best cycling performance ever achieved for Li|LAGP|Li cells with various electrode/electrolyte interlayers operating at room temperature (Table S1 in the ESM). The LAGP pellet cycled for 1,600 h remained intact with a clean and smooth surface (Fig. 4(b)). The SEM images show no signs of metallic Li or side reaction products (Fig. 4(c) and Fig. S3(c) in the ESM). Neither XPS (Fig. 4(d)) nor XRD (Fig. S8 in the ESM) detected any change in surface oxidation state or crystal phase.

The high performance of this hybrid interlayer is a direct result of its composition. The LiTFSI/PVCA polymer electrolyte effectively reduces the interfacial resistance between Li and LAGP, but is not sufficient to prevent the side reaction from developing during cycling. The incorporation of SiO_2 fillers in the hybrid interlayer improves chemical stability on top of the good ionic conductivity and mechanical flexibility of the polymer electrolyte. The chemically inert SiO_2 submicrospheres create a physical barrier between Li and LAGP and successfully avoid electrical contact (Fig. 4(e)). The SiO_2 component may also alleviate Li dendrite formation because of its mechanical strength [49, 50]. In addition, the use of SiO_2 significantly lowers the amount of polymer electrolytes needed to form an interlayer and therefore improves its thermal stability. A polymer electrolyte interlayer often requires about 17 μL·cm^{-2} of gel polymer to wet the Li/ceramic interface [51] and more to ensure a good dendrite suppression capability [44]. The existence of a large amount of gel polymer electrolyte can compromise battery safety due to its thermal instability or even flammability. As an inert additive, the SiO_2 submicrospheres not only occupy space in the polymer matrix and reduce the polymer concentration, but can also form a protective barrier during combustion to increase char-forming ability and isolate the polymer from oxygen and heat through a "tortuous path" effect [52], which improves flame retardancy. We tested the stability of PVCA–SiO_2, PVCA, and VC (with LiTFSI) in flame for a few seconds. Expectedly, liquid VC is highly combustible (Figs. S9(a) and S9(b) and Movie ESM1, Part S1 in the ESM). PVCA did not catch fire (Figs. S9(c) and S9(d) and Movie ESM1, Part S2 in the ESM), but shrank and deformed significantly (Fig. S9(e) in the ESM). PVCA–SiO_2 is neither flammable (Figs. S9(f) and S9(g) and Movie ESM1, Part S3 in the ESM) nor easily deformable (Fig. S9(h) in the ESM), making it a desirable interlayer for all-solid-state batteries.

Our PVCA–SiO_2 hybrid interlayer can also function well at the cathode/electrolyte interface to enable all-solid-state full-cell batteries. To demonstrate this, we used $LiFePO_4$ (LFP) as the cathode material and constructed a Li|PVCA–SiO_2|LAGP|PVCA–SiO_2|LFP cell (Fig. S10(a) in the ESM). Cycled at 0.075 mA·cm^{-2} (25 mA·g^{-1} for LFP), the cell exhibited an initial discharge capacity of 153 mA·h·g^{-1} (for LFP) and relatively stable charging and discharging for 100 cycles (Fig. 5). The overpotential is about 125 mV, of which about 50 mV is contributed by the anode and the rest is from the cathode. No obvious increase in overpotential was observed for the first 20 cycles (Fig. S10(b) in the ESM), again confirming that the PVCA–SiO_2 interlayer provides a stable electrode/electrolyte interface. In comparison, the Li|PVCA|LAGP|PVCA|LFP cell with the PVCA polymer electrolyte as interlayers showed an initial capacity of 144 mA·h·g^{-1} and the capacity started to rapidly decay after approximately 65 cycles (Fig. 5). The LFP|LAGP|Li cell (with a tiny amount of carbonate electrolyte wetting the LAGP/LFP interface and with no interlayer at the Li/LAGP interface) showed an even lower initial capacity of 91 mA·h·g^{-1} and a short life of only 20 cycles (Fig. 5).

In conclusion, we have developed a LiTFSI/PVCA–SiO_2 inorganic/polymer hybrid interlayer for LAGP-based all-solid-state Li metal batteries. With high ionic conductivity, low interfacial resistance, mechanical strength, and flame retardancy, this interlayer enables 1,500 h of Li plating/stripping at room temperature.

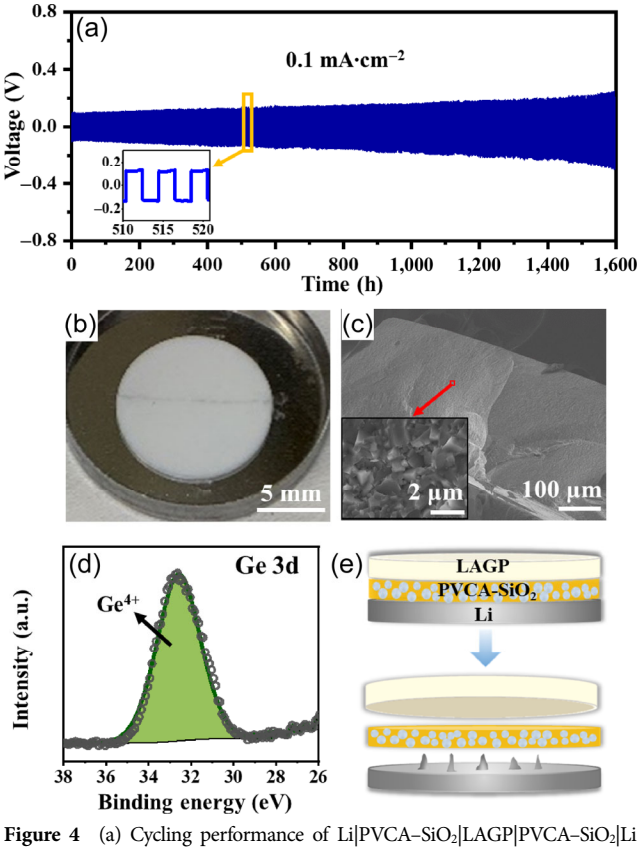

Figure 4 (a) Cycling performance of Li|PVCA–SiO_2|LAGP|PVCA–SiO_2|Li symmetric cell at 0.1 mA·cm^{-2} (current density)-0.1 mA·h·cm^{-2} (capacity). (b) Photograph of the LAGP pellet from the Li|PVCA–SiO_2|LAGP|PVCA–SiO_2|Li cell after 1,600 h of cycling at 0.1 mA·cm^{-2} (current density)-0.1 mA·h·cm^{-2} (capacity). (c) Low-magnification and (inset) magnified SEM images of a cross section of the cycled pellet. (d) Ge 3d XPS of the surface of the cycled LAGP pellet. (e) Schematic illustration of PVCA–SiO_2 interlayer stabilizing Li/LAGP interface.

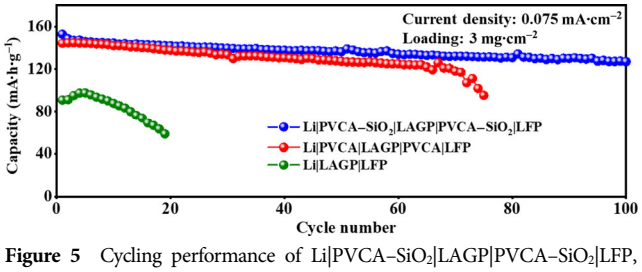

Figure 5 Cycling performance of Li|PVCA–SiO_2|LAGP|PVCA–SiO_2|LFP, Li|PVCA|LAGP| PVCA|LFP, and Li|LAGP|LFP batteries at 0.075 mA·cm^{-2}.

Acknowledgements

This work was supported by the US National Science Foundation (No. CBET-1903342). Y. R. H. acknowledges the exchange graduate student scholarship from the China Scholarship Council. Y. R. Z. acknowledges the Link Foundation Energy Fellowship. L. M. Q. acknowledges support from the Ministry of Science and Technology of China (No. 2018YFA0703502). H. L. W. acknowledges the Sloan Research Fellowship.

Electronic Supplementary Material: Supplementary material (experimental details, additional data, and movie of flammability tests) is available in the online version of this article at https://doi.org/10.1007/s12274-020-2993-4.

References

[1] Tikekar, M. D.; Choudhury, S.; Tu, Z. Y.; Archer, L. A. Design principles for electrolytes and interfaces for stable lithium-metal batteries. *Nat. Energy* **2016**, *1*, 16114.

[2] Manthiram, A.; Yu, X. W.; Wang, S. F. Lithium battery chemistries enabled by solid-state electrolytes. *Nat. Rev. Mater.* **2017**, *2*, 16103.

[3] Xu, X. X.; Wen, Z. Y.; Wu, X. W.; Yang, X. L.; Gu, Z. H. Lithium ion-conducting glass-ceramics of $Li_{1.5}Al_{0.5}Ge_{1.5}(PO_4)_3$-$x$ Li_2O (x = 0.0–0.20) with good electrical and electrochemical properties. *J. Am. Chem. Soc.* **2007**, *90*, 2802–2806.

[4] Zhao, E. Q.; Ma, F. R.; Guo, Y. D.; Jin, Y. C. Stable LATP/LAGP double-layer solid electrolyte prepared via a simple dry-pressing method for solid state lithium ion batteries. *RSC Adv.* **2016**, *6*, 92579–92585.

[5] Bu, J. F.; Leung, P.; Huang, C.; Lee, S. H.; Grant, P. S. Co-spray printing of $LiFePO_4$ and PEO-$Li_{1.5}Al_{0.5}Ge_{1.5}(PO_4)_3$ hybrid electrodes for all-solid-state Li-ion battery applications. *J. Mater. Chem. A* **2019**, *7*, 19094–19103.

[6] Peng, J.; Wu, L. N.; Lin, J. X.; Shi, C. G.; Fan, J. J.; Chen, L. B.; Dai, P.; Huang, L.; Li, J. T.; Sun, S. G. A solid-state dendrite-free lithium-metal battery with improved electrode interphase and ion conductivity enhanced by a bifunctional solid plasticizer. *J. Mater. Chem. A* **2019**, *7*, 19565–19572.

[7] Wang, X.; Zhai, H. W.; Qie, B. Y.; Cheng, Q.; Li, A. J.; Borovilas, J.; Xu, B. Q.; Shi, C. M.; Jin, T. W.; Liao, X. B. et al. Rechargeable solid-state lithium metal batteries with vertically aligned ceramic nanoparticle/polymer composite electrolyte. *Nano Energy* **2019**, *60*, 205–212.

[8] Kamaya, N.; Homma, K.; Yamakawa, Y.; Hirayama, M.; Kanno, R.; Yonemura, M.; Kamiyama, T.; Kato, Y.; Hama, S.; Kawamoto, K. et al. A lithium superionic conductor. *Nat. Mater.* **2011**, *10*, 682–686.

[9] Han, F. D.; Zhu, Y. Z.; He, X. F.; Mo, Y. F.; Wang, C. S. Electrochemical stability of $Li_{10}GeP_2S_{12}$ and $Li_7La_3Zr_2O_{12}$ solid electrolytes. *Adv. Energy Mater.* **2016**, *6*, 1501590.

[10] Mizuno, F.; Hayashi, A.; Tadanaga, K.; Tatsumisago, M. New, Highly ion-conductive crystals precipitated from Li_2S-P_2S_5 glasses. *Adv. Mater.* **2005**, *17*, 918–921.

[11] Gao, Z. H.; Sun, H. B.; Fu, L.; Ye, F. L.; Zhang, Y.; Luo, W.; Huang, Y. H. Promises, challenges, and recent progress of inorganic solid-state electrolytes for all-solid-state lithium batteries. *Adv. Mater.* **2018**, *30*, 1705702.

[12] Inaguma, Y.; Chen, L. Q.; Itoh, M.; Nakamura, T. Candidate compounds with perovskite structure for high lithium ionic conductivity. *Solid State Ionics* **1994**, *70–71*, 196–202.

[13] Li, Y. T.; Zhou, W. D.; Xin, S.; Li, S.; Zhu, J. L.; Lü, X. J.; Cui, Z. M.; Jia, Q. X.; Zhou, J. S.; Zhao, Y. S. et al. Fluorine-doped antiperovskite electrolyte for all-solid-state lithium-ion batteries. *Angew. Chem., Int. Ed.* **2016**, *55*, 9965–9968.

[14] Fu, K.; Gong, Y. H.; Liu, B. Y.; Zhu, Y. Z.; Xu, S. M.; Yao, Y. G.; Luo, W.; Wang, C. W.; Lacey, S. D.; Dai, J. Q. et al. Toward garnet electrolyte-based Li metal batteries: An ultrathin, highly effective, artificial solid-state electrolyte/metallic Li interface. *Sci. Adv.* **2017**, *3*, e1601659.

[15] Han, X. G.; Gong, Y. H.; Fu, K.; He, X. F.; Hitz, G. T.; Dai, J. Q.; Pearse, A.; Liu, B. Y.; Wang, H.; Rubloff, G. et al. Negating interfacial impedance in garnet-based solid-state Li metal batteries. *Nat. Mater.* **2017**, *16*, 572–579.

[16] Chen, L.; Li, Y. T.; Li, S. P.; Fan, L. Z.; Nan, C. W.; Goodenough, J. B. PEO/garnet composite electrolytes for solid-state lithium batteries: From "ceramic-in-polymer" to "polymer-in-ceramic". *Nano Energy* **2018**, *46*, 176–184.

[17] Zhong, Y. R.; Xie, Y. J.; Hwang, S.; Wang, Q.; Cha, J. J.; Su, D.; Wang, H. L. Highly efficient all-solid-state lithium/electrolyte interface induced by an energetic reaction. *Angew. Chem., Int. Ed.*, in press, DOI: 10.1002/anie.202004477.

[18] Porz, L.; Swamy, T.; Sheldon, B. W.; Rettenwander, D.; Frömling, T.; Thaman, H. L.; Berendts, S.; Uecker, R.; Carter, W. C.; Chiang, Y. M. Mechanism of lithium metal penetration through inorganic solid electrolytes. *Adv. Energy Mater.* **2017**, *7*, 1701003.

[19] Han, F. D.; Westover, A. S.; Yue, J.; Fan, X. L.; Wang, F.; Chi, M. F.; Leonard, D. N.; Dudney, N. J.; Wang, H.; Wang, C. S. High electronic conductivity as the origin of lithium dendrite formation within solid electrolytes. *Nat. Energy* **2019**, *4*, 187–196.

[20] Richards, W. D.; Miara, L. J.; Wang, Y.; Kim, J. C.; Ceder, G. Interface stability in solid-state batteries. *Chem. Mater.* **2016**, *28*, 266–273.

[21] Wang, C. H.; Sun, Q.; Liu, Y. L.; Zhao, Y.; Li, X.; Lin, X. T.; Banis, M. N.; Li, M. S.; Li, W. H.; Adair, K. R. et al. Boosting the performance of lithium batteries with solid-liquid hybrid electrolytes: Interfacial properties and effects of liquid electrolytes. *Nano Energy* **2018**, *48*, 35–43.

[22] Key, B.; Schroeder, D. J.; Ingram, B. J.; Vaughey, J. T. Solution-based synthesis and characterization of lithium-ion conducting phosphate ceramics for lithium metal batteries. *Chem. Mater.* **2012**, *24*, 287–293.

[23] Liang, J. Y.; Zeng, X. X.; Zhang, X. D.; Zuo, T. T.; Yan, M.; Yin, Y. X.; Shi, J. L.; Wu, X. W.; Guo, Y. G.; Wan, L. J. Engineering janus interfaces of ceramic electrolyte via distinct functional polymers for stable high-voltage Li-metal batteries. *J. Am. Chem. Soc.* **2019**, *141*, 9165–9169.

[24] Zhang, M.; Huang, Z.; Cheng, J. F.; Yamamoto, O.; Imanishi, N.; Chi, B.; Pu, J.; Li, J. Solid state lithium ionic conducting thin film $Li_{1.4}Al_{0.4}Ge_{1.6}(PO_4)_3$ prepared by tape casting. *J. Alloy Compd.* **2014**, *590*, 147–152.

[25] Wang, L. Y.; Hu, S. M.; Su, J. M.; Huang, T.; Yu, A. S. Self-sacrificed interface-based on the flexible composite electrolyte for high-performance all-solid-state lithium batteries. *ACS Appl. Mater. Interfaces* **2019**, *11*, 42715–42721.

[26] Jung, Y. C.; Park, M. S.; Doh, C. H.; Kim, D. W. Organic-inorganic hybrid solid electrolytes for solid-state lithium cells operating at room temperature. *Electrochim. Acta* **2016**, *218*, 271–277.

[27] Zhang, Q. Q.; Ding, F.; Sun, W. B.; Sang, L. Preparation of LAGP/P(VDF-HFP) polymer electrolytes for Li-ion batteries. *RSC Adv.* **2015**, *5*, 65395–65401.

[28] Wang, C. H.; Bai, G. L.; Yang, Y. F.; Liu, X. J.; Shao, H. X. Dendrite-free all-solid-state lithium batteries with lithium phosphorous oxynitride-modified lithium metal anode and composite solid electrolytes. *Nano Res.* **2019**, *12*, 217–223.

[29] Wang, C. H.; Yang, Y. F.; Liu, X. J.; Zhong, H.; Xu, H.; Xu, Z. B.; Shao, H. X.; Ding, F. Suppression of lithium dendrite formation by using LAGP-PEO (LiTFSI) composite solid electrolyte and lithium metal anode modified by PEO (LiTFSI) in all-solid-state lithium batteries. *ACS. Appl. Mater. Interfaces* **2017**, *9*, 13694–13702.

[30] Wang, S.; Wang, J.; Liu, J. J.; Song, H. C.; Liu, Y. J.; Wang, P. F.; He, P.; Xu, J.; Zhou, H. S. Ultra-fine surface solid-state electrolytes for long cycle life all-solid-state lithium-air batteries. *J. Mater. Chem. A* **2018**, *6*, 21248–21254.

[31] Lewis, J. A.; Cortes, F. J. Q.; Boebinger, M. G.; Tippens, J.; Marchese, T. S.; Kondekar, N.; Liu, X. M.; Chi, M. F.; McDowell, M. T. Interphase morphology between a solid-state electrolyte and lithium controls cell failure. *ACS Energy Lett.* **2019**, *4*, 591–599.

[32] He, L. C.; Sun, Q. M.; Chen, C.; Oh, J. A. S.; Sun, J. G.; Li, M. C.; Tu, W. Q.; Zhou, H. H.; Zeng, K. Y.; Lu, L. Failure mechanism and interface engineering for NASICON-structured all-solid-state lithium metal batteries. *ACS. Appl. Mater. Interfaces* **2019**, *11*, 20895–20904.

[33] Lee, W.; Lyon, C. K.; Seo, J. H.; Lopez-Hallman, R.; Leng, Y. J.; Wang, C. Y.; Hickner, M. A.; Randall, C. A.; Gomez, E. D. Ceramic-salt composite electrolytes from cold sintering. *Adv. Funct. Mater.* **2019**, *29*, 1807872.

[34] Chung, H.; Kang, B. Mechanical and thermal failure induced by contact between a $Li_{1.5}Al_{0.5}Ge_{1.5}(PO_4)_3$ solid electrolyte and Li metal

in an all solid-state Li cell. *Chem*. *Mater*. **2017**, *29*, 8611–8619.

[35] Meesala, Y.; Chen, C. Y.; Jena, A.; Liao, Y. K.; Hu, S. F.; Chang, H.; Liu, R. S. All-solid-state Li-ion battery using $Li_{1.5}Al_{0.5}Ge_{1.5}(PO_4)_3$ as electrolyte without polymer interfacial adhesion. *J*. *Phys*. *Chem*. *C* **2018**, *122*, 14383–14389.

[36] Dong, D. R.; Zhou, B.; Sun, Y. F.; Zhang, H.; Zhong, G. M.; Dong, Q. Y.; Fu, F.; Qian, H.; Lin, Z. Y.; Lu, D. R. et al. Polymer electrolyte glue: A universal interfacial modification strategy for all-solid-state Li batteries. *Nano Lett*. **2019**, *19*, 2343–2349.

[37] Zhou, Y. C.; Li, Z. J.; Lu, Y. C. A stable lithium-selenium interface via solid/liquid hybrid electrolytes: Blocking polyselenides and suppressing lithium dendrite. *Nano Energy* **2017**, *39*, 554–561.

[38] Liu, Y. J.; Li, C.; Li, B. J.; Song, H. C.; Cheng, Z.; Chen, M. R.; He, P.; Zhou, H. S. Germanium thin film protected lithium aluminum germanium phosphate for solid-state Li batteries. *Adv*. *Energy Mater*. **2018**, *8*, 1702374.

[39] Liu, Y. L.; Sun, Q.; Zhao, Y.; Wang, B. Q.; Kaghazchi, P.; Adair, K. R.; Li, R. Y.; Zhang, C.; Liu, J. R.; Kuo, L. Y. et al. Stabilizing the interface of NASICON solid electrolyte against Li metal with atomic layer deposition. *ACS Appl*. *Mater*. *Interfaces* **2018**, *10*, 31240–31248.

[40] Cortes, F. J. Q.; Lewis, J. A.; Tippens, J.; Marchese, T. S.; McDowell, M. T. How metallic protection layers extend the lifetime of NASICON-based solid-state lithium batteries. *J*. *Electrochem*. *Soc*. **2019**, *167*, 050502.

[41] Liu, J. Y.; Liu, T.; Pu, Y. J.; Guan, M. M.; Tang, Z. Y.; Ding, F.; Xu, Z. B.; Li, Y. Facile synthesis of NASICON-type $Li_{1.3}Al_{0.3}Ti_{1.7}(PO_4)_3$ solid electrolyte and its application for enhanced cyclic performance in lithium ion batteries through the introduction of an artificial Li_3PO_4 SEI layer. *RSC Adv*. **2017**, *7*, 46545–46552.

[42] Wang, L. D. Y.; Liu, D.; Huang, T.; Geng, Z.; Yu, A. S. Reducing interfacial resistance of a $Li_{1.5}Al_{0.5}Ge_{1.5}(PO_4)_3$ solid electrolyte/electrode interface by polymer interlayer protection. *RSC Adv*. **2020**, *10*, 10038–10045.

[43] Yu, Q. P.; Han, D.; Lu, Q. W.; He, Y. B.; Li, S.; Liu, Q.; Han, C. P.; Kang, F. Y.; Li, B. H. Constructing effective interfaces for $Li_{1.5}Al_{0.5}Ge_{1.5}(PO_4)_3$ pellets to achieve room-temperature hybrid solid-state lithium metal batteries. *ACS Appl*. *Mater*. *Interfaces* **2019**, *11*, 9911–9918.

[44] Zhou, W. D.; Wang, S. F.; Li, Y. T.; Xin, S.; Manthiram, A.; Goodenough, J. B. Plating a dendrite-free lithium anode with a polymer/ceramic/polymer sandwich electrolyte. *J*. *Am*. *Chem*. *Soc*. **2016**, *138*, 9385–9388.

[45] Li, W. W.; Wang, Q.; Jin, J.; Li, Y. P.; Wu, M. F.; Wen, Z. Y. Constructing dual interfacial modification by synergetic electronic and ionic conductors: Toward high-performance LAGP-based Li-S batteries. *Energy Storage Mater*. **2019**, *23*, 299–305.

[46] Zhang, Z. H.; Zhao, Y. R.; Chen, S. J.; Xie, D. J.; Yao, X. Y.; Cui, P.; Xu, X. X. An advanced construction strategy of all-solid-state lithium batteries with excellent interfacial compatibility and ultralong cycle life. *J*. *Mater*. *Chem*. *A* **2017**, *5*, 16984–16993.

[47] Chai, J. C.; Liu, Z. H.; Ma, J.; Wang, J.; Liu, X. C.; Liu, H. S.; Zhang, J. J.; Cui, G. L.; Chen, L. Q. *In situ* generation of poly (vinylene carbonate) based solid electrolyte with interfacial stability for $LiCoO_2$ lithium batteries. *Adv*. *Sci*. **2017**, *4*, 1600377.

[48] Stöber, W.; Fink, A.; Bohn, E. Controlled growth of monodisperse silica spheres in the micron size range. *J*. *Colloid Interface Sci*. **1968**, *26*, 62–69.

[49] Zhou, D.; Liu, R. L.; He, Y. B.; Li, F. Y.; Liu, M.; Li, B. H.; Yang, Q. H.; Cai, Q.; Kang, F. Y. SiO_2 hollow nanosphere-based composite solid electrolyte for lithium metal batteries to suppress lithium dendrite growth and enhance cycle life. *Adv*. *Energy Mater*. **2016**, *6*, 1502214.

[50] Pan, Q. W.; Smith, D. M.; Qi, H.; Wang, S. J.; Li, C. Y. Hybrid electrolytes with controlled network structures for lithium metal batteries. *Adv*. *Mater*. **2015**, *27*, 5995–6001.

[51] Liu, Q.; Yu, Q. P.; Li, S.; Wang, S. W.; Zhang, L. H.; Cai, B. Y.; Zhou, D.; Li, B. H. Safe LAGP-based all solid-state Li metal batteries with plastic super-conductive interlayer enabled by in-situ solidification. *Energy Storage Mater*. **2020**, *25*, 613–620.

[52] Kashiwagi, T.; Gilman, J. W.; Butler, K. M.; Harris, R. H.; Shields, J. R.; Asano, A. Flame retardant mechanism of silica gel/silica. *Fire Mater*. **2000**, *24*, 277–289.